CHARACTERIZATION OF ACOUSTIC MODES IN AEROENGINES

by

MICHELLE OTERO
B.S. University of Central Florida, 2018

A thesis submitted in partial fulfillment of the requirements
for the degree of Master of Science
in the Department of Mechanical and Aerospace Engineering
in the College of Engineering and Computer Science
at the University of Central Florida
Orlando, Florida

Fall Term
2018

Major Professor: Kareem Ahmed

ABSTRACT

Acoustic instabilities remain a key design concern faced in the development of liquid rocket engines. The interaction between the acoustic modes and the occurring combustion reactions can be detrimental to the engine. The fluctuating pressure waves resulting from the flame oscillations in the system can potentially lead to engine failure. For this reason, research in acoustic instabilities and methods to minimize the influences on the engine, has maintain interest in the aerospace community. The scope of this study was to design, optimize and characterize acoustic behaviors of a scaled rocket combustion chamber simulating acoustic pressure waves. Tangential and longitudinal acoustic waves of the system were extracted and validated through analytical and computational fluids dynamics models. The results of this study will assist with the process of extracting dominant oscillation frequencies of a system essential in the design of acoustic suppression devices for attenuation of critical frequencies.

I would like to dedicate my Master Thesis to my best friend and older sister Ammy Patino. You have always been my number one fan and motivator throughout my academic journey. Special thanks to my family and freinds who are my second family. These past couples of years wouldn't be the same without all of you.

ACKNOWLEDGMENTS

I would like to acknowledge my advisor Dr. Kareem Ahmed, for his guidance throughout this process and Siemens for providing the funds for my research. I would also like to thank all my fellow graduate students in PERL for helping me, especially Wilmer Flores.

TABLE OF CONTENTS

LIST OF FIGURES

LIST OF TABLES

CHAPTER ONE: INTRODUCTION

Combustion instabilities experienced by rocket engines dates to the early days of the rocket community. These instabilities are known to cause extensive even detrimental damages to engines due to prolong pressure oscillations that substance high temperature seen by the chamber walls. As a key factor in the performance of rocket engines, combustion instabilities have been studied widely for decades. Understanding the physical phenomenon of this occurrence is of essential importance to minimum its impact on rocket engines. The work presented focuses on the development of a diagnostic technique used to predict accurately acoustic amplification in real combustors and develop a baseline behavior of acoustic modes found in an annular chamber. The following paragraphs will include general background knowledge in combustion instabilities, primarily in thermoacoustic instabilities and the acoustics oscillations behind the phenomenon. This thesis will focus on the development of a new technique to accurately extract dominate oscillations in a system.

1.1 Background

Instabilities in combustion can be broken down into three different categories; Intrinsic, system and chamber instabilities [1]. Intrinsic instabilities are results of natural occurrences such as Rayleigh-Taylor instabilities and chemical kinetic instabilities. These events occur regardless of combustion process in the engines. System instabilities, comprises of instabilities resulting from the interaction between the combustion in the system and other components of the system. Lastly, there is chamber instabilities, which is a result directly from the combustion occurring in the chamber such as shock and thermoacoustic instabilities.

Since the 1950s', thermoacoustic instabilities has been of immense interest, being a root cause in combustion instabilities seen in rocket engines. Thermoacoustic instabilities is the result of the coupling between natural acoustic modes of a system and the combustion occurring. These interaction results in a feedback loop as illustrated in Figure 1. As fuel and air are introduce, pressure in the chamber causes mixture's inhomogeneity. As a result, there occurs an unsteady heat release, which acts as an acoustic source that propagates sound disturbances within the system. The disturbances reflect once they experience an acoustic boundary, interacting with the flame. This interaction causes local perturbations in the flow velocity and increases the fluctuation in the heat release rate. When the perturbations couple with the acoustic modes present, the acoustic disturbance grows in amplitude and increase the instabilities experience by the system[2]–[7].

Natural acoustic instability modes present in a chamber are link to the design of the chamber itself. These fundamental instabilities can be classified as either longitudinal and transverse and will be described in detail in the next section. Investigating how to control these acoustic excitation is an important research goal for both designers and theoreticians [8].

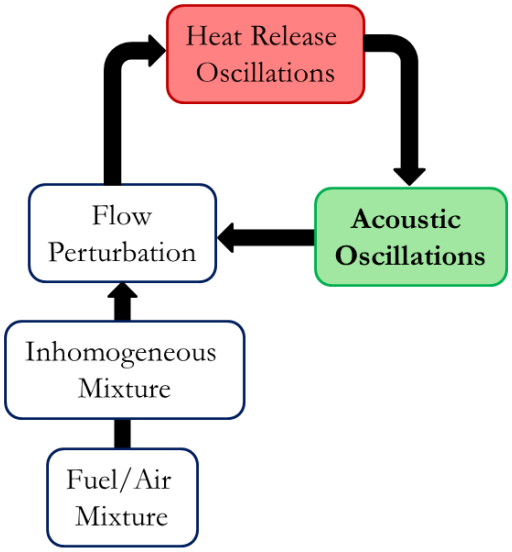

Figure 1: Thermoacoustic Instability Coupling Feedback Loop

1.2 Longitudinal Instabilities

Longitudinal modes are defined by the length of the combustion chamber. The acoustic pressure waves associated to longitudinal modes travel in the axial direction parallel to the displacement of the medium. The cross-sectional geometry of the chamber has no influence on the propagation of the acoustic wave. The location of the dominate frequency of longitudinal modes are controlled by the speed of sound of the medium and the length of the chamber [9], [10]. Applying the proper boundaries to Equation 1, the natural frequency of a longitudinal mode of a half wave can be computed.

$$f_L = \frac{l \cdot c}{2 \cdot L_C} \tag{1}$$

where l is the longitudinal mode (ie. 1,2,3), c is the speed of sound and L_C is the axial length of the chamber. In rocket engines, longitudinal modes are not critical due to the natural dissipation of them due to the geometry of the nozzle [11]–[14].

1.3 Transverse Instabilities

Due to the nature of their oscillation behavior, transverse waves are seen extremely dangers to the components in a combustion chamber [5], [8], [11]–[19]. Unlike Longitudinal modes, the acoustic pressure wave in transverse waves travel perpendicular to the propagation of the medium. Their maximum acoustic pressure amplitude happens at the wall with zero pressure at the center. These acoustic pressure waves are controlled by the cross-sectional geometry of the chamber. In a rectangular system, the transverse modes behave relatively the same. In a cylinder chamber, these modes can either act tangentially or radially.

Acoustic modes with tangential behaviors are can be classified as spinning or standing tangential modes. The acoustic pressure wave associated to the tangential mode propagates in the clockwise and counterclockwise direction in an annular chamber. When rotation occurs, the tangential mode is considered a spinning mode. Spinning modes have pressure nodes diving the chamber circumferentially and they that rotate with the speed of sound. A standing wave occurs when two spinning pressure waves rotate in the opposite direction and cancel each other net energy. The pressure nodes present in a standing wave, divides the chamber circumferentially but are stationary [12], [20]. Detecting motion of the tangential mode is critical for design aspects of

modern engines. understanding the mechanism allows for development of devices to suppress the mode accordingly.

To compute analytically the natural frequency of a transverse mode, Equation 2, can be utilized.

$$f_{M,N} = \frac{\alpha_{M,N} \cdot c}{2 \cdot \pi \cdot r} \quad (2)$$

where M,N index the tangential and radial mode respectively, α is the Bessel function of the mode and r is the radius of the chamber.

1.4 Literature

Although dominate modes are determined by the specific engine design, the physical mechanism behind it remains the same. Research in acoustic oscillations and thermoacoustic instabilities can date back to the late decades. In the 1800s, Rayleigh discovered the fundamental phenomenon of thermoacoustic. Through experimentation, he recognized the relationship between heat and acoustic vibration. His demonstration consisting of a hydrogen flame burning in an open tube, where the gas expansion coupled with the natural vibration of the tube and created “singing flames”. These singing flames were a representation of the gas expansion in phase with the natural resonance of the tube, producing self-excitation vibrations [21]. The combustion of the flame provided the energy needed to sustain the vibration experienced inside the tube. Rayleigh defined a criterion for thermoacoustic instabilities that are still used in modern rocket combustion chamber designs. His criteria shown in Equation 3, is the inequality of the perturbation in pressure and the heat release compared to the wave energy dissipation through time [21], [22].

$$\int_0^{\tau}\int_0^{V} p'(x,t)q'(x,t)dvdt > \int_0^{\tau}\int_0^{V} \phi(x,t)dvdt \quad (3)$$

With p and q representing the perturbation in pressure and heat release respectively. τ V and ϕ are the period of oscillation, control volume and the wave energy dissipation [22].

Laudien et al 1994, Natanzon and Culick 1999, were pioneers in the numerical model for a rocker combustion chamber. By solving the wave equation with the appropriate boundary conditions to a combustion chamber, Laudien et al, developed the numerical model shown to calculate theoretical natural frequencies modes in a chamber. The combustion chamber in this model is treated as a closed/closed system although the nozzle prevents a fully closed system [11], [23], [24]. Equation 4 is the adaptation of the closed/closed cylindrical equation to rocket combustion chambers.

$$f_{l,m,n} = \frac{c}{2\pi}\sqrt{\left(\frac{\lambda_{mn}^2}{R_c^2}+\frac{l^2\pi^2}{L_c^2}\right)} \quad (4)$$

where λ is the Bessel function coefficient corresponding to the desired transverse mode listed in Table 1. The L_C and R_C are the chamber length and radius respectively. To account for the geometrical contraction due to the conical frustum, the chamber length (L_C) is replaced by the effective chamber length (L_E). Laudien, refers to the effective length as the distance between the faceplate and the nozzle throat less approximately one-half of the converging nozzle length [11].

Much work was theoretical based and focused on liner analysis of these instabilities [3], [25], [26]. As a linear phenomenon the disturbances were considered, linearly unstable, linearly stable and neutral stable. Although the behavior was ideal, it is not physically possible. additional

research has risen to answer questions physical behavior. Nonlinear analysis research investigated oscillatory behavior theoretically and numerically [14], [27]–[29]. Experimental research has increase throughout the year; Lee et al investigated the theoretical models derived from Laudien and implemented acoustic attenuation devices to improve engine conditions [13]. Poinsot et al, developed a technique to identify azimuthal modes in annular combustion chamber [30] in 2011. Latest research was conducted by Sirignano et al, developing a 2D model for transverse combustion instabilities in a combustion chamber [31]

CHAPTER TWO: EXPERIMENTAL APPROACH

2.1 Experimental Facility

The acoustic rig consists of various components to investigate the acoustic modes in a combustion chamber. The model combustion chamber consists of an annular PVC pipe with an inner diameter of 330.2 mm and a total combustor length of 268 mm as shown in Figure 2. To simulate engine behavior, the chamber was designed has an open-closed system. A 12.7 mm thick solid acrylic plate is attached upstream of the chamber and an acrylic conical frustum is attached downstream of the chamber. The conical frustum has a lower base diameter of 330.20 mm and an upper base diameter of 190.50 mm. To ensure similarity to rocket engines, the conical frustum has an included angle of 60 degrees and a length of 132 mm.

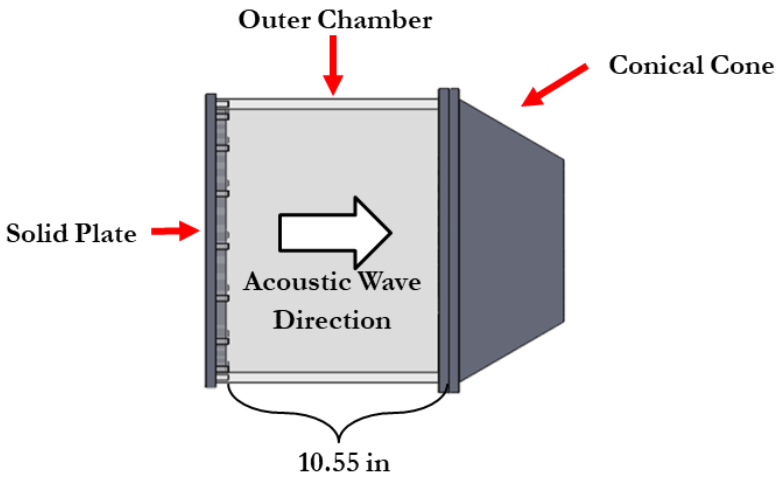

Figure 2: Combustor Simplification Schematic

Eight speakers were inserted into the model chamber wall. Eight JL Audio C5-400 speakers were located 25 mm downstream from the inner faceplate. All were installed with the same

separation distance, consisting of 45° on center with each speaker. This allows for an even distribution of the acoustic sounds induced in the system. The layout of the speakers can be seen in Figure 3. The speakers where chosen for their bandwidth, ranging from 300Hz to 5000Hz. The frequencies of interest range from 400Hz to 1800Hz, placing them within the optimal range of the speakers. A Pyle ProPTA1000 amplifier was utilized to amplify the power of the acoustic signal and provide an even distribution of the acoustic sound in the system. To acquire data for the acoustic mode map, the speaker directly opposite from the top row of microphones is used. For damping purpose, the remaining speakers are covered from within with a rubber material to block the acoustic waves traveling into the speaker housing.

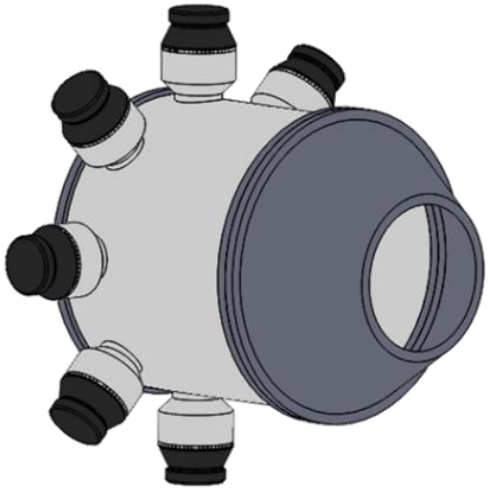

Figure 3: Speakers Placement Schematic

2.2 Acoustic Diagnostic

Sixteen PCB model #378B02 microphones were utilized to capture the acoustic pressures experienced by the system during excitation. They have a sensitivity of 50 mV/pa and a frequency range of 7 to 10000 Hz. The high sensitivity and frequency range helped with the saturation limits

of the microphones. With the microphones placed relatively close to the audio source, noise saturation was of a concern. Four PCB model #482C05 signal conditioners were utilized to amplify the microphone signals for the NI DAQ and LabVIEW.

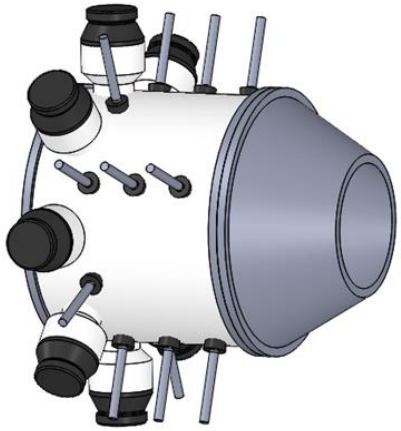

Figure 4: 3D Microphones Location

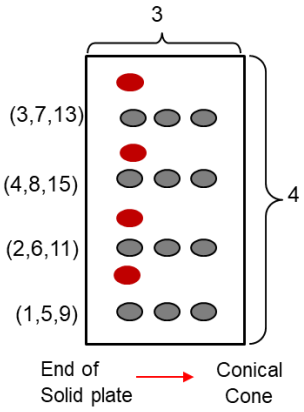

Figure 5: 2D Unwrapped layut of Microphones Location

These microphones were placed strategically to maximum the modes that can be reconstructed. Figure 4 demonstrates the 3D representation of the microphone locations. Following the Nyquist Shannon Theorem, a minimum of 4 microphones were required in the circumferential

direction to capture the 2T mode. A row of 8 microphones were place closed to the speakers to capture the highest or lowest peak of the acoustic mode. Two additional rows of four microphones were spaced evenly between the last set of microphones and the conical frustum. These set of microphones were 72 mm away from one another in the axial direction. Figure 5 demonstrates the 2D unwrapped version of the microphone locations for a better understanding. As the images shows the locations of the microphones with assist with the visualization of the beginning, middle and end of the acoustic mode. In addition, the microphones setup will permit for simultaneous capture of longitudinal and tangential modes. To isolate the microphones from external vibration excitation, rubber stoppers were utilized. The material and thickness of the stopper, absorbed any vibration due to external excitation. The complete experimental setup is detailed in Figure 6.

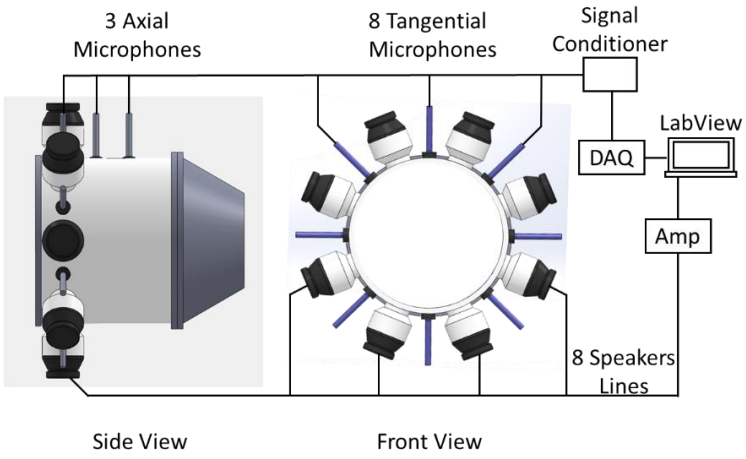

Figure 6: Full Schematic of Experimental Facility

2.3 Experimental Procedures

2.3.1 Acoustic Mode and Phase Analysis

An acoustic soundwave was induced in the system to simulate flame oscillations. The acoustic sound induced in the system was a continuous sine sweep ranging from 150Hz to 2200Hz. The frequencies of interest were ranging between 400 and 1600Hz, and having a sine sweep safely below and above the range, ensured the frequencies of interest were in the stable audio power region of the sweep. Figure 7, illustrates the power level vs the frequency analysis of the sine sweep file used for this work. As shown with the vertical lines, the frequencies of interested fell in the constant power level region. A LabVIEW program was coded to simultaneously play the continuous sine sweep and record the voltage excitation within the system.

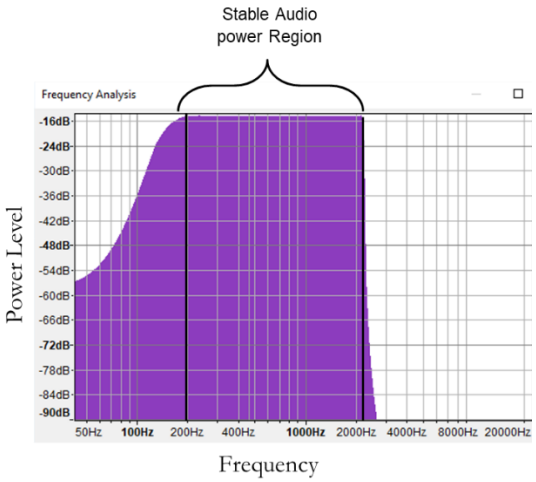

Figure 7: Power Level vs Frequency Analysis of Sinusoidal Sweep

Two different tests were required to fully capture the varies mode behaviors in the system. Due to quick dissipation from the 1L mode, to have the capability to capture the mode, the conical frustum had to be closed as shown in Figure 8. This allowed for the mode to remain inside the chamber and provide enough time for the microphones to capture the voltage excitation. Once that

test was completed, the second set of data was taken with the conical frustum opened as shown in Figure 9. Utilizing the data from the open-closed configuration, the 1T 1T1L 2T and 2T1L modes were extracted.

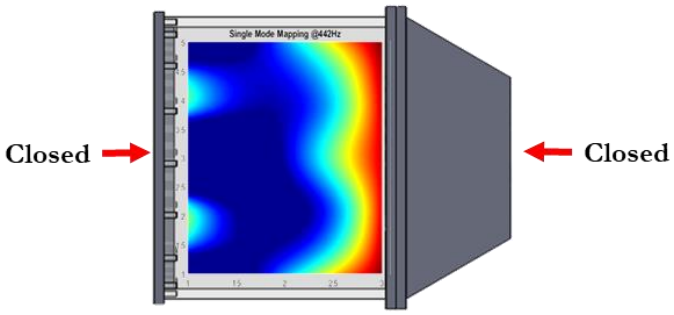

Figure 8: Closed -Closed Chamber Configuration Setu

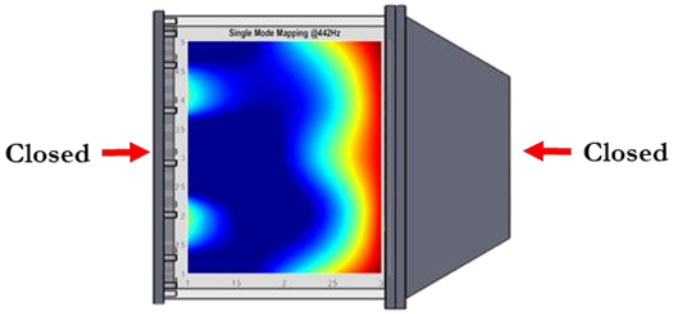

Figure 9: Open- Closed Chmaber Configuration Setup

With the possibility of standing and spinning tangential modes, the cross-spectrum power density (CPSD) of the microphones in the circumference distance was computed. The phase between the microphones were extracted from the CPSD. The data acquire for the mode map analyze was utilized to compute the CPSD.

3.2.2 Decay Measurements

After the dominate modes were extracted from the data, decay measurements were taken. To perform this task, the constant acoustic tone of the interested frequency was played for 5 second. After the five second, the audio was abruptly shut off and the decay rate of the oscillating pressures were recorded. These measurements are essential for creating a baseline for the damping present prior to anything noise attenuation devices integrated to the system.

CHAPTER THREE: RESULTS AND DISCUSSION

3.1 Theoretical Calculations

Laudien et al, studies describe the interior acoustic behavior of a chamber has a closed-closed system although the chamber is open through the nozzle. The five natural frequencies associated with the acoustic modes of the chamber were computed using the mathematical equation (1).where λ is the Bessel function coefficient corresponding to the desired transverse mode listed in Table 1. The L_C and R_C are the chamber length and radius respectively. To account for the geometrical contraction due to the conical frustum, the chamber length (L_C) is replaced by the effective chamber length (L_E). Laudien, refers to the effective length as the distance between the faceplate and the nozzle throat less approximately one-half of the converging nozzle length [7]. Effective acoustic length for the chamber in this work is the distance from the inner faceplate of the acrylic solid plate and the midway point of the conical frustum. The five analytical natural frequencies are shown in Table 1.

Table 1: Eigenfrequencies(Theoretical)

Acoustic Mode	Orthogonal Directions k	m	N	λ Transversal	Theoretical Frequency, Hz
1L	1	0	0	0	443
1T	0	1	0	1.8412	604
1T1L	1	1	0	0	750
2T	0	2	0	3.0542	1002
2T1L	1	2	0	0	1308

3.2 Acoustic Mode Shape

Pressure tomographic reconstruction is used to visualize and identify dominate acoustic oscillations modes in the system. Figure 10, displays the power spectral density (PSD) of the

excitation voltage during the closed-closed configuration test to capture the 1L mode. The PSD represents the intensity of the fluctuation occurring in the chamber. The dominate frequencies shown in the PSD correspond to longitudinal and tangential modes. The first peak amplitude appears at 442 Hz, reconstruction of tomographic intensity image exhibits a 1L mode. Tomography display in figure 8, shows of the mode amplitude validates that natural frequency of the 1L mode.

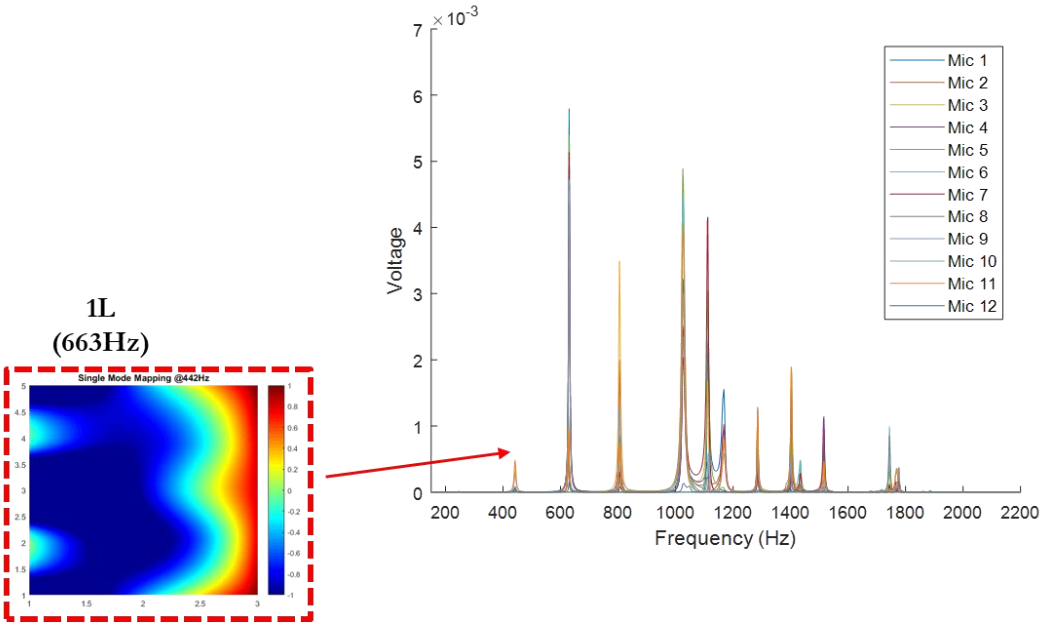

Figure 10: Mode Map Behavior for Closed-Closed Configuration

The modes 1T to 2T1L were extracted from the open-closed case measurements. The PSD plot does not have a 1L appear, this is attributed to the speed of longitudinal mode moving out of the chamber. The 1L acoustic mode leaves the chamber quickly and the microphone setup does not pick up the associated amplitudes. Limitations to the DAQ and microphone sampling rates do not permit the intensity information to be recorded quick enough. The open-closed configuration PSD as well as mode tomography is shown in figure 11. Comparison from figure 10 and 11, the modes ranging from 1T to 2T1L are seen in both PSD, with a higher amplitude in figure 8, due to the

closure of the conical frustum. This closure increased the volume experienced inside the chamber, increasing the amplitude of the signals captured by the microphones.

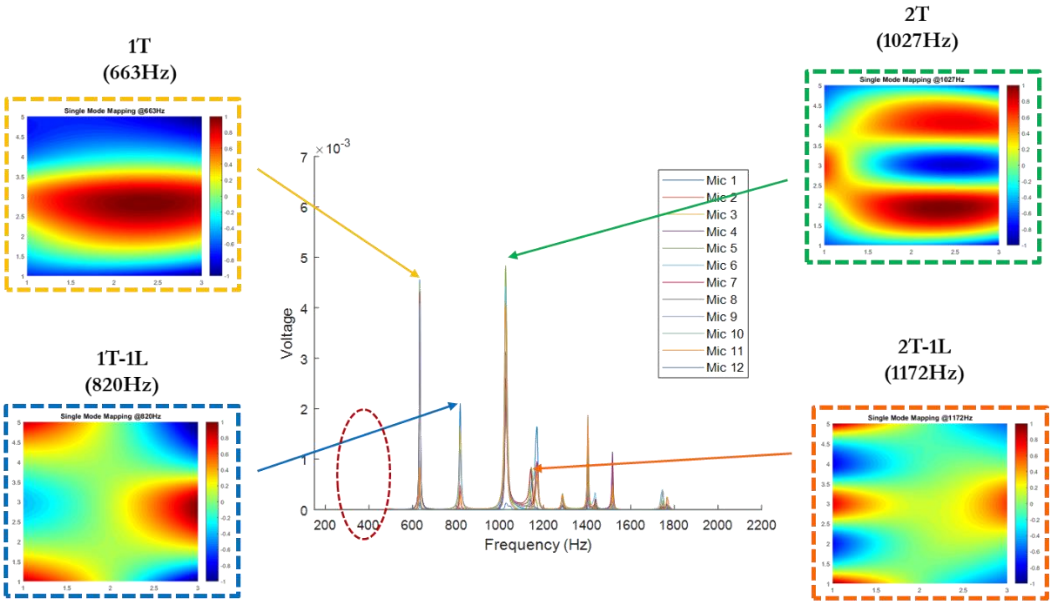

Figure 11: Open-Closed Configuration PSD and Tomography

Tomographic images of longitudinal, tangential, and a combination of the two are observed throughout the chambers excited frequency range. Microphone layout captures 1L up to 2T1L modes, additional peaks are observed in the PSD plot. Potential modes such as radial or higher order longitudinal and tangential modes outside of the mode range are expected to follow. It is apparent more modes exist but have not been identified due to the number of microphones installed into the chamber. To capture a specific mode in either single direction or combined, it is important to use Nyquist-Shannon theorem for necessary microphone layout in both directions along chamber. The number of microphones required to find any single mode is 2 times the mode, 2T would need 4 total microphones in the tangential direction to perform reconstruction of mode correctly. Higher oscillatory frequency modes up to 3T2L would require 6 tangential and 4

longitudinal microphones arrangement to appropriately distinguish modes. Hence, a 12-microphone layout has limitations that are observed to be at 2T1L mode reconstruction. From the measurements taken, table 2 lays out the natural frequencies associated with their corresponding mode.

Table 2: Theorectical and Experimental Values

Acoustic Mode	Theoretical Frequency, Hz	Experimental Frequency, Hz
1L	443	442
1T	604	663
1T1L	750	820
2T	1002	1027
2T1L	1308	1172

3.3 Phase Analysis

Additional analysis of the phase angle for tangential and combined mode comparisons aid in distinguishing a behavior of whether the mode appears to be a standing or spinning. To further characterize existing modes in an acoustic chamber establishing phase angle associates a mode to either a standing wave or spinning wave. Applying a cross-spectral power density (CPSD) determines the phase angle for mode behavior. Figures 12a-d, display the phase angles for modes extracted from the modal chamber. The 1T phase angle first shows various negative peaks from 0 to π which cross beyond the zero axis, signifying directional motion of the mode. However, intensity values of microphones are opposite of those found from π to 2π, indicating a positive motion in the opposite direction. Combining intensity data of the two halves from the modal chamber represent two opposing directional forces which cancel each other, demonstrating a

standing mode that pulses and is motionless. A 1T standing waves propagates axially outwards of the modal chamber due to no bias in phase angle. Bias shifts in angles characterize spinning wave behavior for modes with a bias phase angle direction it is observed either have a clockwise or counter-clockwise acoustic pressure wave. Modes 1T through 2T1L have standing wave mode features which is attributed to the cancelation of phase angle intensities. Phase analysis of the demonstrates the number of peaks identifying the intensity of 1T compared to 2T. The 2T and 2T1L standing modes have two positive or negative peaks, the opposing differences are related to the recorded time. Phase angle with only a single peak on either the positive or negative side show only a single peak. Peak information expresses whether the mode would be a longitudinal or tangential mode.

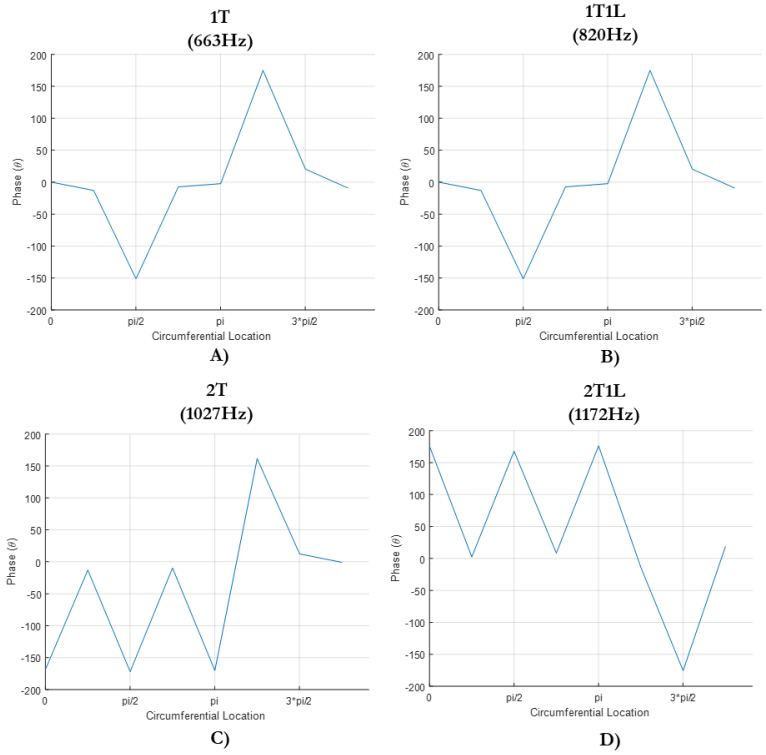

Figure 12: Phase Analysis of Modes 1T to 2T1L

3.4 COMSOL Validation

Reconstruction images from COMSOL assist validate experimental data tomography. Range of selected modes are highlights in figure XX and displayed up to 2T1L. Proving the intensity structure of each mode at the specific location is determined to agree with each mode found within the PSD plot. A COMSOL simulation is utilized to ensure modes experienced in modal chamber are similar that of experimental measurements. Experimental data may demonstrate differences in mode peaks, indicating shifts of mode peak locations for computational data are shown to shift in the power spectral density (PSD). Slight frequency shifts occur due to differences from CAD model and actual fabricated chamber finish. Chamber sealing is crucial to maintain air mass control volume in the system, promoting mode frequencies to appear at identical locations.

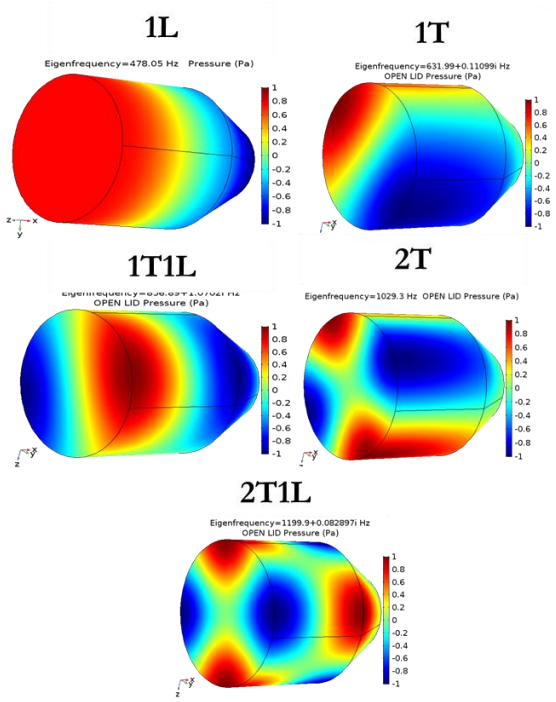

Figure 13: COMSOL Simulations

Figure 13, shows the COMSOL modes found in the chamber design. Tomographic images display similar acoustic intensity amplitudes compared experimental data. COMSOL simulation is a useful tool to calibrate according to experimental measurements recorded in modal chamber. It provides insight of system effects to mode and decay analysis as components are changed. Differing drawing model specifications for example such as the speaker PVC housing proves greater damping transpires from a larger volume design. PVC housing resonance frequency dampens mode amplitudes found within investigated bandwidth, reductions to the PVC housing volume changes resonance frequency to a higher frequency. Removal of the damping behavior of the PVC housing is ideal for eliminating influences on the system, design recommendations are to equip chamber with surface mounted speakers that follow the contour of the chamber. Frequency locations for 1L, 1T, and 1T1L were observed to have a percent difference of 4%. Minor differences are experienced between the simulation and experimental modes recognized in the modal chamber. Each COMSOL mode is found to be in agreeance with the theoretical and experimental measurements identified in combustor chamber as shown in the graph in Figure 14.

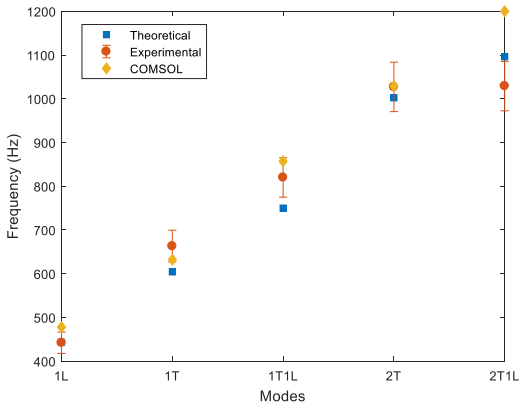

Figure 14: Natural Frequencies Comparisons

3.5 Decay Measurements

Mode decay rates were characterized for the developmental of future attenuation devices. An empty combustors decay rates serve as baseline data that would be compared towards alternative suppression devices decay measurements. From scaling the chamber, it is possible to calculate modes for a different combustor. Figure 15 is an image of the 1L to 2T1L amplitude with respect to time.

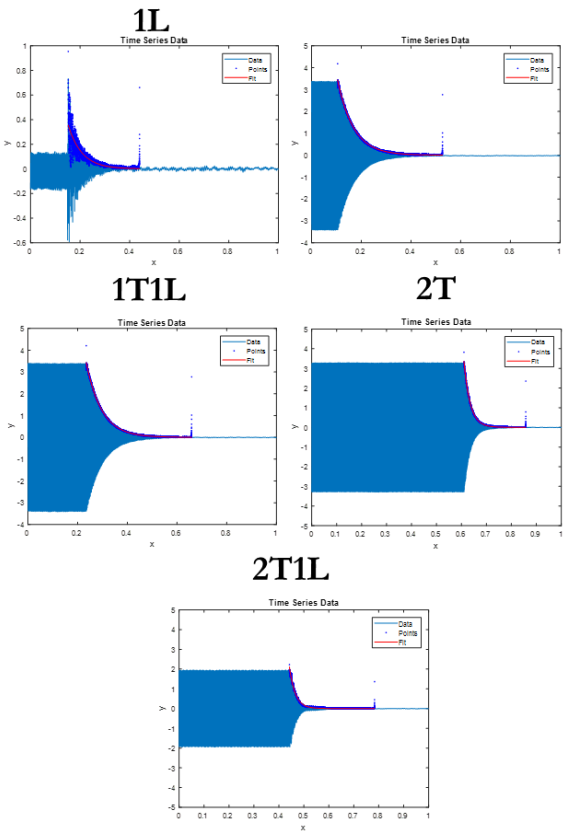

Figure 15: Decay Measurements 1L to 2T1L

Decay rate post processing is performed through selection of the highest peak before the frequency signal dissipates out of system within milliseconds. Figure 16, expresses decay rate

order of modes selected from modal chamber. Longitudinal modes are observed to decay quickest and tangential modes demonstrate to be the slowest to dissipate. When analyzing a combinational mode such as 1T1L, it accounts for mode features producing a decay time of 62ms that exists between a 57 ms for 1L and 68 ms for 1T. Higher order modes follow the correct order but present even quicker dissipation times, this is attributed to the PVC speaker housing that dampens mode intensities that exist near the 1200Hz. The associated resonance frequency of the PVC housing is observed to affect the amplitude. Decay time order for the higher frequencies accurately follows the expected trend were 2T has a longer decay time compared to the 2T1L combined mode.

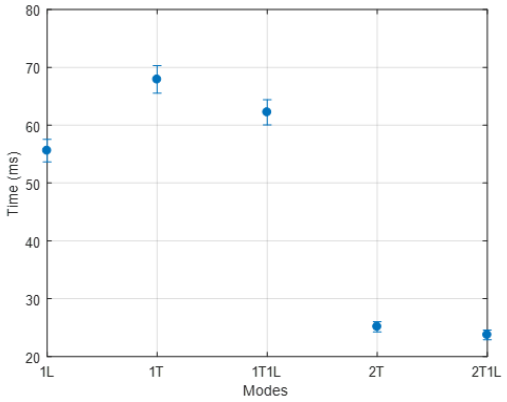

Figure 16: Comparison of Decay Rates

CHAPTER FOUR: CONCLUSION

This research focused on designing a facility that would have the capability to capture longitudinal and tangential modes simultaneously. The main objective was to characterize the facility behavior to match previous work and establish acoustic behaviors in chamber like environment. The experiments were performed in a non-reacting auditory test environment with a sinusoidal sweep emulating longitudinal and tangential modes in the system.

Using raw voltage, a PSD of the system was obtained and the dominate oscillation frequencies were extracted. To capture the first five acoustic modes of the system, two cases were taken, a closed-closed and open-closed case. The closed-closed setup consisted of both ends of the chamber closed. This allow for the complete capture of the 1L mode amplitude while the open-closed setup captured the remaining modes. 1L mode naturally having low amplitudes due to quick dissipation, closing the conical frustum helped with storing the energy inside the chamber long enough for the microphones to capture the mode oscillation. The tangential mode was the strongest mode present as predicted in the PSD. Each dominate frequency were reconstructed using the data recorded from the 12 microphones in the chamber and the acoustic pressure behavior were examined. CPSD was used to determine the rotation of the tangential modes in the system. Finally, The dominate eigenfrequencies of the system were validated with COMSOL simulation.

The decay rate measurement of the varies acoustic modes, followed expected trends. The longitudinal modes dissipated the quickest from the chamber compared to their corresponding tangential mode. When coupled with the longitudinal mode, the tangential modes' decay rate

increased slightly. Issues were seen in the results for the 2T and 2T1L decay rate measurement but were concluded to be associated to the natural resonate frequency of the speaker's housing.

Future work will include investigate in noise attenuation devices. The data from this work can be scaled to determine the baseline acoustic behavior in a chamber. The longitudinal frequencies can scale based on the desired length of the chamber and the tangential frequencies can scale associating the radius of the chamber. The speed of sound and temperature associated to the system will shift the frequencies directly.

REFERENCES

[1] W. Anderson and V. Yang, *Liquid rocket engine combustion instability*. 1995.

[2] F. Culick and P. Kuentzmann, "Unsteady motions in combustion chambers for propulsion systems," 2006.

[3] D. Harrje, "Liquid propellant rocket combustion instability," 1972.

[4] Z. Zhang, D. Zhao, S. Li, C. Ji, X. Li, J. L.- Energy, and undefined 2015, "Transient energy growth of acoustic disturbances in triggering self-sustained thermoacoustic oscillations," *Elsevier*.

[5] H. Hubbard, "Aeroacoustics of flight vehicles: Theory and practice. volume 1. noise sources," 1991.

[6] W. Krebs, P. Flohr, B. Prade, and S. Hoffmann, "Thermoacoustic stability chart for high intensity," *Combust. Sci. Technol.*, vol. 174, no. 7, pp. 99–128, 2002.

[7] C. Huynh, A. Ghafourian, S. Mahalingam, J. V. V Daily, C. H. A. Ghafourian, S. Mahalingam, and J. W. Daily, "AIAA 92-0465 COMBUSTOR DESIGN FOR ATOMIZATION STUDY IN LIQUID ROCKET ENGINES University of Colorado Boulder , Colorado 80309-0427."

[8] O. M. Umurhan, "Exploration of fundamental matters of acoustic instabilities in combustion chambers," *Cent. Turbul. Res. Annu. Res. Briefs*, pp. 99–108, 1999.

[9] M. Oschwald and B. Knapp, "Investigation of the combustion chamber acoustics and its interaction with LOX/H2 spray flames," *Prog. Propuls. Phys.*, vol. 1, pp. 243–262, 2009.

[10] M. S. S. A. Santana Jr. P. T. Lacava., and L. C. S. Góes, “Acoustic cavities design procedures,” *Therm. Eng.*, vol. 6, no. December, pp. 27–33, 2007.

[11] Laudien E., Pongratz R., Pierro P., and Prelick D., “Experimental procedures aiding the design of acoustic cavities,” *Liq. Rocket Combust. Instab.*, pp. 377–399, 1995.

[12] J. W. Bennewitz and R. A. Frederick, “Overview of Combustion Instabilities in Liquid Rocket Engines - Coupling Mechanisms & Control Techniques,” *49th AIAA/ASME/SAE/ASEE Jt. Propuls. Conf.*, no. December 2017, 2013.

[13] K. J. Lee, H. J. Kim, S. Seo, and H. S. Choi, “Experimental Verification for Acoustic Damping Enhancement by Gaps in Injector-Formed Baffles,” *J. Propuls. Power*, vol. 25, no. 2, pp. 435–442, 2009.

[14] V. Yang, J. Wicker, M. Y.-L. rocket engine combustion, and undefined 1995, “Acoustic waves in combustion chambers,” *arc.aiaa.org*.

[15] M. Turner, *Rocket and spacecraft propulsion: principles, practice and new developments*. 2008.

[16] A. Oyediran and B. Park, “Review of Combustion-Acoustic,” 2018.

[17] M. L. Dranovsky, *Combustion Instabilities in Liquid Rocket Engines*. Reston ,VA: American Institute of Aeronautics and Astronautics, 2007.

[18] J. C. OEFELEIN and V. YANG, “Comprehensive review of liquid-propellant combustion instabilities in F-1 engines,” *J. Propuls. Power*, vol. 9, no. 5, pp. 657–677, Sep. 1993.

[19] G. P. (George P. Sutton and O. Biblarz, *Rocket propulsion elements*. .

[20] A. Pozarlik, “Vibro-acoustical instabilities induced by combustion dynamics in gas turbine combustors,” 2010.

[21] L. R.-R. I. Proc. and undefined 1878, “The explanation of certain acoustical phenomena,” *ci.nii.ac.jp*.

[22] J. Rayleigh, *The theory of sound*. 1896.

[23] R. Pirk, C. d. A. Souto, D. D. da Silveira, C. M. de Souza, and L. C. S. Góes, “Liquid rocket combustion chamber acoustic characterization,” *J. Aerosp. Technol. Manag.*, vol. 2, no. 3, pp. 269–278, 2010.

[24] R. Pirk, C. D’Andrade Souto, T. Barbosa de Araújo, and D. S. De Almeida, “Modeling the Acoustic Behavior of a Liquid Rocket Combustion Chamber At Room and Operational,” *23rd ABCM Int. Congr. Mech. Eng. December 6-11, 2015, Rio Janeiro, RJ, Brazil*, no. December, 2015.

[25] L. Crocco and S. Cheng, “Theory of combustion instability in liquid propellant rocket motors,” 1956.

[26] F. Culick and V. Yang, “Prediction of the stability of unsteady motions in solid-propellant rocket motors,” 1992.

[27] “On Strong Transverse Waves Without Shocks in a Circular Cylinder,” *J. Aeronaut. Sci.*, vol. 23, no. 6, pp. 583–593, Jun. 1956.

[28] B. Zinn, E. P.-S. (International) on Combustion, and undefined 1971, “Nonlinear combustion instability in liquid-propellant rocket engines,” *Elsevier*.

[29] E. Awad and F. E. C. Culick, “On the Existence and Stability of Limit Cycles for Longitudinal Acoustic Modes in a Combustion Chamber,” *Combust. Sci. Technol.*, vol. 46, no. 3–6, pp. 195–222, 1986.

[30] T. Poinsot, P. Wolf, G. Staffelbach, L. Y. M. Gicquel, and J. D. Muller, “Identification of azimuthal modes in annular combustion chambers,” *Cent. Turbul. Res. Annu. Res. briefs*, no. February, pp. 249–258, 2011.

[31] W. Sirignano, J. Delplanque, … C. C.-L. rocket engine, and undefined 1995, “Liquid-propellant droplet vaporization: a rate controlling process for combustion instability,” *arc.aiaa.org*.